PRECISION MEASUREMENT OF $\sin^2\theta_W$ FROM $\nu - N$ SCATTERING AT NUTEV

Jaehoon Yu
Department of Physics
University of Texas, Arlington, TX76019

Representing the NuTeV Collaboration

ABSTRACT

We present the final result for $\sin^2\theta_W$ from the $\nu - N$ deep inelastic scattering experiment, NuTeV, at Fermilab. This measurement of $\sin^2\theta_W$ is the result of measuring the ratio of neutral to charged current cross sections in neutrino and anti-neutrino beams separately. The resulting value of $sin^2\theta_W^{(on-shell)}$ from this measurement is $0.2277 \pm 0.0013(\text{stat}) \pm 0.0009(\text{syst})$. This value is equivalent to the mass of the W boson, $M_W = 80.14 \pm 0.08\text{GeV/c}^2$. The value of $\sin^2\theta_W$ is about three standard deviations higher than the Standard Model prediction.

1 Introduction

The Standard Model[1] (SM) of particle physics unifies the weak and electromagnetic interactions to $\mathrm{SU(2)} \times \mathrm{U_Y(1)}$ gauge theory. The theory introduces weak neutral current interactions to unify the electrically neutral portion of the interactions and uses measured physical parameters, such as:

$$g^{'} = gtan\theta_W, \tag{1}$$

$$e = gsin\theta_W, \tag{2}$$

$$G_F = \frac{g^2\sqrt{2}}{8M_W^2}, \tag{3}$$

$$\frac{M_W}{M_Z} = cos\theta_W, \tag{4}$$

to relate to mixing parameters for the couplings. Neutrinos in this picture are unique because they only interact through left-handed weak interactions, probing the weak sector only, therevy reducing complications in the measurements. Therefore, neutrino interactions provide clean channel for probing weak interactions. Since in the electroweak sector of the Standard Model it is not known *a priori* what the mixture of electrically neutral electromagnetic and weak mediators is, the mixing parameter $\sin^2\theta_W$ provides the degree of this mixing.

As it has been shown in Eqs. 1–4, within the on-shell renormalization scheme, $\sin^2\theta_W$ is:

$$sin^2\theta_W^{on-shell} = 1 - \frac{M_W^2}{M_Z^2}. \tag{5}$$

Therefore, a measurement of $\sin^2\theta_W$ also provides information on mass of the W boson (M_W), within the context of SM and using the precisely measured value of Z boson mass (M_Z). Since M_W is a fundamental parameter in the electroweak sector of SM, the other parameters; Fermi constant (G_F), the fine structure constant (α), mass of the Z boson (M_Z), and electroweak radiative correction δr can be expressed in terms of M_W. Among these parameters G_F, α_{EM}, and M_Z are measured to very high precision. Since the precision of M_W from the $\sin^2\theta_W$ measured in neutrino experiments is at a comparable level of direct measurements from collider experiments, the indirect measurement of M_W can be used to constrain the mass of SM Higgs bosons, M_H, together with the measured top quark mass via radiative corrections.

In addition, since $\sin^2\theta_W$ measures light quark couplings, it is sensitive to other

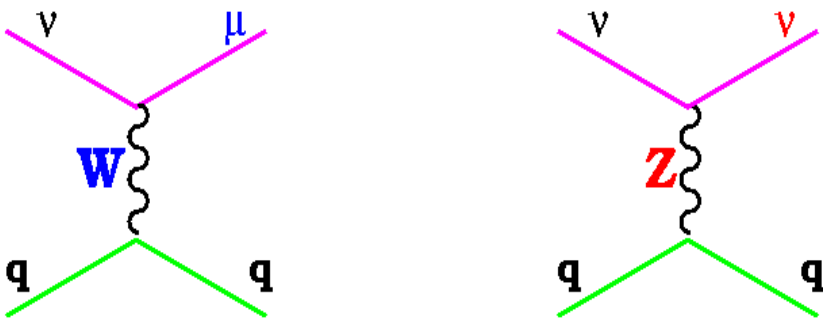

Figure 1: Feynman diagrams of CC (left) and NC (right) interactions for ν_μ ($\overline{\nu}_\mu$).

types of couplings, such as anomalous couplings. In other words, due to the radiative corrections that requires modification with the introduction of new particles, precision measurement of $\sin^2\theta_W$ also provides a constraint on new physics beyond the SM, including new vector bosons, quark compositeness, neutrino oscillations, etc.

In this paper, we present the final result for the $\sin^2\theta_W$ measurement, a possible interpretation of the deviation of this measurement from the SM prediction, and the resulting mass of the W boson from the $\nu - N$ DIS experiment, NuTeV,[2] at Fermilab.

2 Measurement of $\sin^2\theta_W$ in $\nu - N$ DIS

In tree level calculations, the electroweak mixing angle, $\sin^2\theta_W$, appears in neutral current interactions of neutrinos, and the calculations have process dependent radiative corrections. As can be seen in Fig. 1, since the cross section of CC interactions of neutrinos is proportional to weak isospins ($I^{(3)}_{Weak}$) while that for NC interactions is proportional to ($I^{(3)}_{Weak} - Q_{EM}\sin^2\theta_W$), the ratio of the CC to NC cross sections is proportional to $\sin^2\theta_W$, as expressed in the Llewellyn-Smith formula[3]:

$$\mathcal{R}^{\nu(\overline{\nu})} = \frac{\sigma^{\nu(\overline{\nu})}_{NC}}{\sigma^{\nu(\overline{\nu})}_{CC}} = \rho^2\left(\frac{1}{2} - \sin^2\theta_W + \frac{5}{9}\sin^4\theta_W\left(1 + \frac{\sigma^{\overline{\nu}(\nu)}_{CC}}{\sigma^{\nu(\overline{\nu})}_{CC}}\right)\right). \quad (6)$$

Previous experiments have exploited this relationship to measure $\sin^2\theta_W$ through the measurement of the ratio between NC and CC cross sections. Since experi-

ments measure the ratio of the number of NC and CC-like events, some corrections are necessary to extract $\sin^2\theta_W$ from the measured ratio. The radiative corrections are needed to take into account radiations through strong and electroweak interactions. Corrections for heavy quark effects are needed to take into account heavy quark production threshold effects. Isovector target corrections are needed because the iron in the calorimeter that is used as neutrino target has an imbalance in the number of neutron and protons in the atom. In addition, higher order corrections, such as higher twist effects and longitudinal structure function effects, are needed.

3 Previous Measurement of $\nu - N$ DIS

Since neutrinos interact only through weak interactions, their cross sections are extremely small ($\mathcal{O}(10^{-38})\mathrm{cm}^2/\mathrm{GeV}$). Neutrino experiments traditionally use various techniques to obtain a sufficient number of statistics. The techniques include; 1) increasing the number of protons striking the primary target to produce a large number of secondary hardons (π and K), thereby resulting in a large number of neutrinos; 2) inncreasing the energy of neutrinos to increase cross sections; and 3) using dense material as the target for neutrinos to interact in. In this section, I will describe the setup for a neutrino experiment designed to measure $\sin^2\theta_W$ precisely and point out the systematic uncertainties that the measurement encountered. Next we motivate the need for upgrades to the NuTeV experiment and detail the improvements made in the experiment.

3.1 Neutrino Beam Production

Figure 2 shows a schematic diagram of CCFR experiment, the previous incarnation of the NuTeV experiment. As can be seen, the experiment had a straight line configuration from the primary proton target location to the detector. It used a Quadrupole Triplet (QT) magnet train in the region immediately downstream of the primary target to collect as many secondary charged hadrons as possible. The QT train is followed by a few hundred meter vacuum pipe for the secondary hadrons to decay in to produce neutrinos. The decay products are then passed through lead, steel, and dirt shields to filter out any remaining particles other than neutrinos. This beamline chain provides both neutrinos and anti-neutrinos simul-

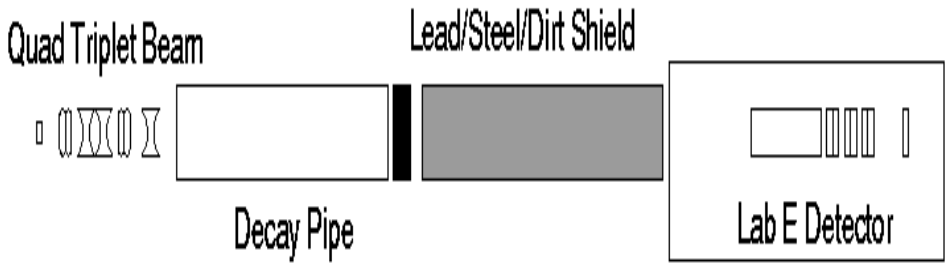

Figure 2: A schematic diagram of CCFR (FNAL-E770) experiment.

taneously. The neutrinos produced from this conventional beamline are mostly muon type neutrinos, ν_μ, with a few percent electron neutrino component.

3.2 Event Separation

The most important element in this measurement is separating NC from CC events as cleanly as possible experimentally. Figure 3 shows event displays for CC and NC events. Since CC events result in a quark and a muon in the final state, there is the long trace of a minimum ionizing particle track through the detector, along with a hadronic shower resulting from materialization of the quark in the event. Conversly, since NC events results in a quark and neutrino in the final state, they do not produce long muon tracks.

Given the characteristics of CC and NC interactions, an experimental variable has been developed to separate CC and NC candidate events. This separation is obtained statistically by using the event length variable. The event length is defined for each event to be the number of counters with energy deposition above 1/4 of that for a single muon. The NC events have a short length due to the absence of the muons in the event, while CC events are long. Figure 4 shows a Monte Carlo (MC) simulation of length distributions for a neutrino (left) and an anti-neutrino beam (right) separately. As can be seen, while the actual CC events predominantly populate longer lengths and the NC events short length regions, there are events that cross over the cut-off value of length, contaminating the precise counting. In addition, there are other type of events, such as CC events resulting from non-zero electron neutrino components, which cannot be distinguished from short NC events.

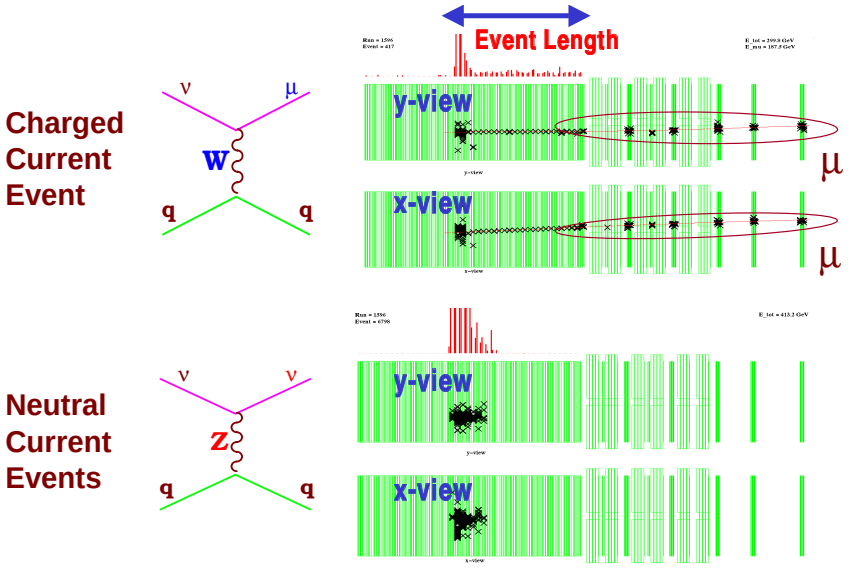

Figure 3: Event displays of CC (top) and NC (bottom) interactions. The CC interactions result in a hadronic shower from a quark and a muon in the events while NC events only have a hadronic shower from the quark.

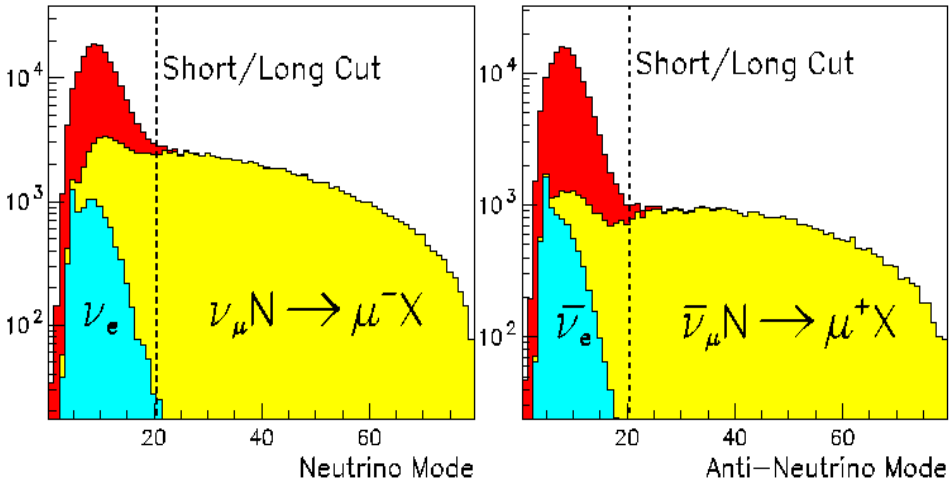

Figure 4: Monte Carlo prediction of length distributions from various sources.

Thus, while the experimentally measured ratio of the number of short events, N_{short}, to the number of long events, N_{long}, $\mathcal{R}_\nu^{exp} = N_{short}/N_{long}$, represents the NC to CC cross section ratio, $\mathcal{R}^{\nu(\overline{\nu})}$, it is necessary for the experiments to use precise MC predictions to correct for contamination. In practice, the experiments vary only the NC couplings in the detailed Monte Carlo (MC), until $\mathcal{R}^{\nu(\overline{\nu})}$ from the MC matches with $\mathcal{R}_\nu^{exp}$.

3.3 Monte Carlo Prediction

The cross section model in the MC incorporates a leading order (LO) corrected Quark-Parton-Model (QPM), using LO parton distribution functions from the CCFR structure function measurements.[4] The second part of the MC simulates detailed detector and beam effects, such as "short" CC events caused by low energy range-out muons or by the muons exiting the detector fiducial volume, "long" NC events due to π/K decays and punch through, electron neutrino (ν_e) CC events which appear short in the detector, and other detector effects that are reflected in the event length variable. The detailed MC also includes various corrections: 1) electromagnetic and electroweak radiative corrections; 2) target isovector effects ($\sim 6\%$ for iron target); 3) higher-order QCD effects due to longitudinal structure functions, R_L[5]; and 4) effects due to heavy quark production.

3.4 Previous Results and Systematic Uncertainties

There are two major sources of systematic uncertainties in the CCFR measurements.[6,7] The first is the theoretical uncertainty due to mass threshold effects in the CC production of charm quarks from the scattering off the sea quarks. This effect is modeled by LO slow-rescaling.[8] The parameters in the slow rescaling model are measured by the CCFR experiment,[9] using events with two oppositely charged muons, where $m_c = 1.31 \pm 0.24\mathrm{GeV/c^2}$ and $\kappa = 0.37 \pm 0.05$. The uncertainties in CC cross section calculations due to the above two parameters result in $\delta\sin^2\theta_W = 0.0027$.

The second source is the lack of precise knowledge about the ν_e flux in the beam. Approximately 80% of the total number of electron neutrinos in the CCFR neutrino beam, which is a mixture of ν and $\overline{\nu}$, come from $K_{e3}^{\pm}$ decays. The ν_e content from this source is well constrained by observed $K_{\mu 2}^{\pm}$ spectra. The remaining 16% of ν_e's come from neutral K decays, K_{Le3}, whose production cross section is

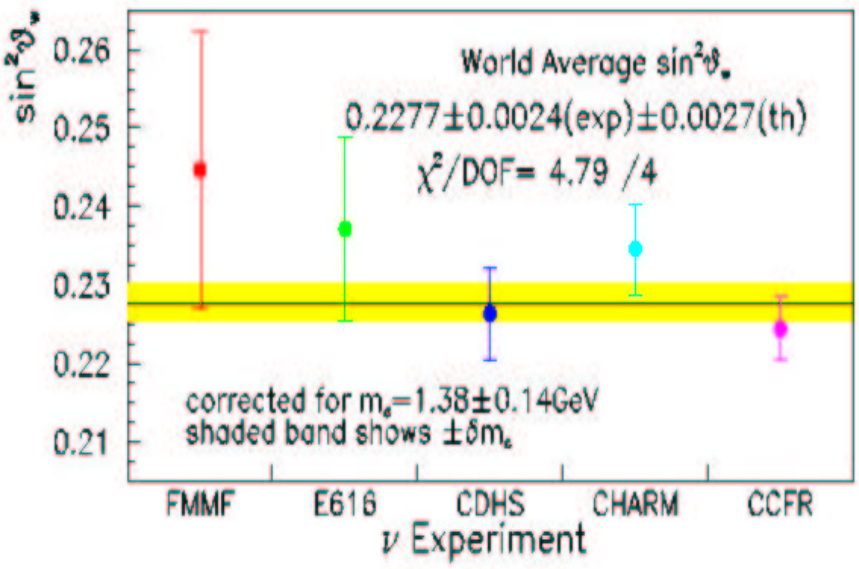

Figure 5: Combined results of $\sin^2\theta_W$ measurements from all previous neutrino experiments.

known to 20% only. These two sources contribute a 4.1% uncertainty to N_{ν_e}, based on a Monte Carlo study. A direct measurement, based on longitudinal shower development,[10] gives a 3.5% uncertainty. Combining these two uncertainties give a 2.9% uncertainty in N_{ν_e}, which results in $\delta\sin^2\theta_W = 0.0015$. Combining all the errors, the final CCFR result[7] was $\sin^2\theta_W = 0.2236 \pm 0.0041$ which corresponds to an on-shell mass of the W boson $M_W = 80.35 \pm 0.21 GeV/c^2$.

Figure 5 shows the combined results of $\sin^2\theta_W$ from previous neutrino experiments. The band represents the correlated systematic uncertainties from CC production of charm quarks due to the uncertainties in mass of the charm quark, m_c, and the corresponding uncertainties in the production cross section modelled by the slow rescaling mechanism. Figure 6 shows Feynman diagrams for CC production of charm quarks, along with NC process diagram that cannot produce any charm quark from valence quark distributions.

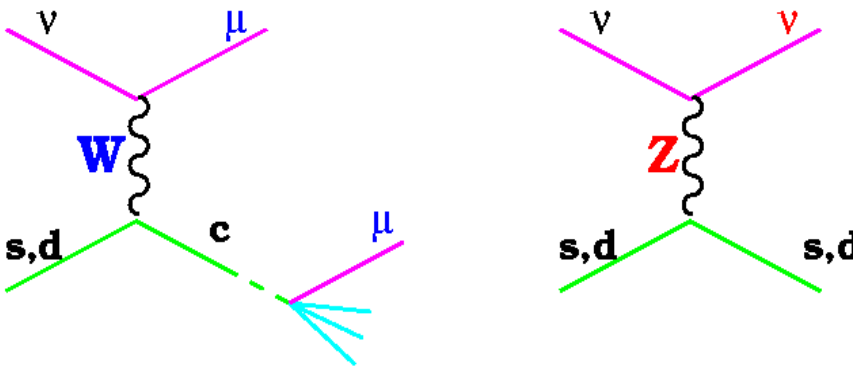

Figure 6: Feynman diagrams for CC production of charm quarks. NC diagram is included to show that NC processes cannot produce charm quarks.

4 Improvements in NuTeV

4.1 Pascos-Wolfenstein Formula

In order to minimize the two largest systematic uncertainties described in the previous section, one needs 1) a technique insensitive to the sea quark distributions, and 2) to minimize the number of electron neutrinos in the beam, especially resulting from K_L. In order to minimize the uncertainty due to charm quark production, NuTeV is designed to use the Paschos-Wolfenstein parameter[11];

$$\mathcal{R}^- = \frac{\sigma^\nu_{NC} - \sigma^{\bar{\nu}}_{NC}}{\sigma^\nu_{CC} - \sigma^{\bar{\nu}}_{CC}} = \frac{R^\nu - rR^{\bar{\nu}}}{1-r} = (g_L^2 - g_R^2) = \rho\left(\frac{1}{2} - \sin^2\theta_W\right). \qquad (7)$$

Since $\sigma^{\nu q} = \sigma^{\bar{\nu}\bar{q}}$ and $\sigma^{\bar{\nu}q} = \sigma^{\nu\bar{q}}$, the effects of scattering off the sea quarks cancel by taking the differences in the neutrino and anti-neutrino cross sections. This technique only leaves only the Cabibbo-suppressed production of heavy quarks from valance u, d and s quarks. However, the measurement of this quantity is complicated due to the fact that the NC final states look identical for ν and $\bar{\nu}$. Thus, in order to use this relationship, one needs to be able to distinguish neutrino NC interactions from anti-neutrino interactions, which can only be achieved by having prior knowledge on the beam.

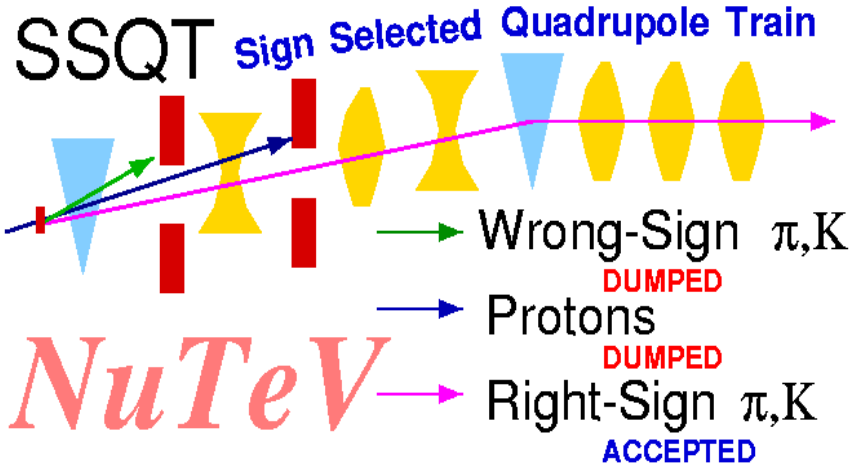

Figure 7: A schematic diagram of the SSQT. The incident proton beam is aimed 7.8 mrad upward relative to the magnet train that follows the primary target.

4.2 Sign-Selected Quadrupole Train

To achieve the discrimination of neutral current interactions, NuTeV modified the beamline to use a Sign-Selected-Quadrupole-Train (SSQT)[12] to select either the ν or $\overline{\nu}$ beam during a given running period. Figure 7 shows a schematic diagram of the SSQT with beam magnet configurations following the primary proton target. The incident proton beam strikes the primary target, consisting of one interaction length of BeO, with an upward incident angle of 7.8 mrad. The target is then followed by a dipole that acts as a charge selector and bends the secondary hadrons with the desired charge onto the horizontal axis, placing them in the direction toward the experiment. At the time of the bend, the neutral hadrons proceed straight ahead while the hadrons with opposite charge bend away from the direction of the detector. This upward incident angle together with a dipole stationed immediately behind the primary target causes the neutral secondary hadrons (especially K_L), opposite charge secondary mesons, and remnant protons to be directly absorbed into the beam dumps in the SSQT. Since the electron neutrino flux from neutral hadron decays is not well measured ($\sim 20\%$ uncertainty), improvement in $\sin^2\theta_W$ uncertainty from this source is significant. The remaining major source of $\nu_e/\overline{\nu}_e$ comes from weak decays of charged kaons, $K^\pm \to \pi^0 e^\pm \nu_e(\overline{\nu}_e)$, the $K^\pm_{e3}$ decays. The contribution from this source has been

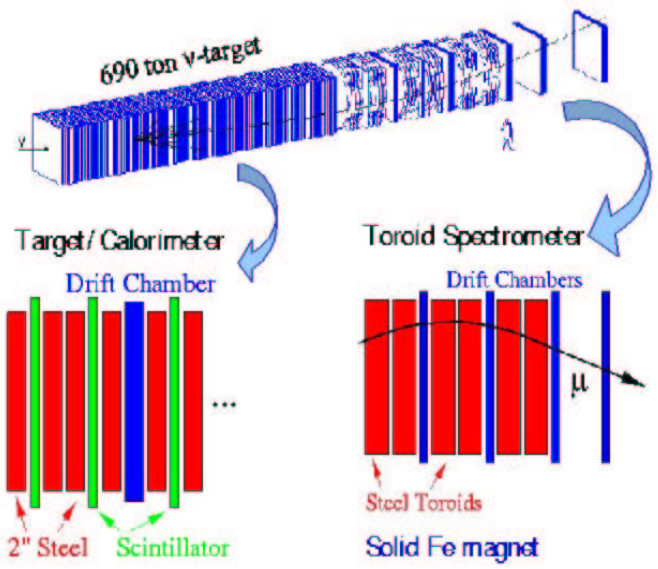

Figure 8: NuTeV detector and the detailed schematic diagrams of its calorimeter array and the muon toroidal spectrometer.

estimated using detailed beam MC. The fractional uncertainty on predictions of $\nu_e/\overline{\nu}_e$ from $K^{\pm}_{e3}$ is $\approx 1.5\%$ and is dominated by the uncertainty in the $K^{\pm}_{e3}$ branching ratio.

4.3 NuTeV Detector

The NuTeV detector consists of a steel/liquid scintillation counter calorimeter that acts as a target to the incoming neutrinos and a muon toroidal spectrometer that follows the calorimeter. The calorimeter has a total of 168 two inch thick steel plates and 84 scintillation counters. The calorimeter is interspersed with 42 drift chambers to provide tracking information for the muons emerging from CC interactions. Figure 8 shows the NuTeV detector and the detailed structures of the calorimeter array and muon toroidal spectrometer. The experiment had a continuous, *in-situ* calibration beam throughout the data taking period. This calibration beam allowed a thorough monitoring of detector response to minimize other experimental systematic uncertainties. Data from the calibration beam also allowed a more realistic simulation of hadronic shower behavior to be used in the analysis, further reducing uncertainties.

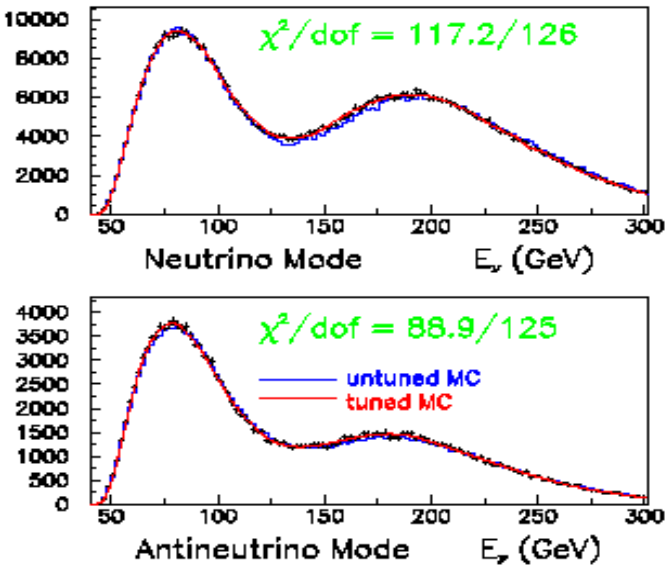

Figure 9: Comparisons of neutrino (top) and anti-neutrino (bottom) fluxes to MC predictions.

The calorimeter hadronic energy resolution[13] measured from the calibration beam is:

$$\frac{\sigma}{E} = A + \frac{50\%}{\sqrt{E}} + \frac{c}{E}. \tag{8}$$

The muon spectrometer momentum resolution is $\Delta p/p \sim 10\%$.

5 NuTeV Data Analysis

The total data sample from the 1996-1997 run corresponds to 1.3×10^{18} protons on target. This section describes the NuTeV $\sin^2\theta_W$ analysis.

5.1 Event Selection Criteria

In order to ensure high vertex finding efficiency and to reduce contamination from cosmic rays, all events are required to have hadronic shower energy, E_{had}, greater than 20 GeV. In addition, to guarantee full containment of hadronic showers and muons and to further reduce events from electron neutrinos, the event vertex was required to be within the central two-thirds of the detector in the trans-

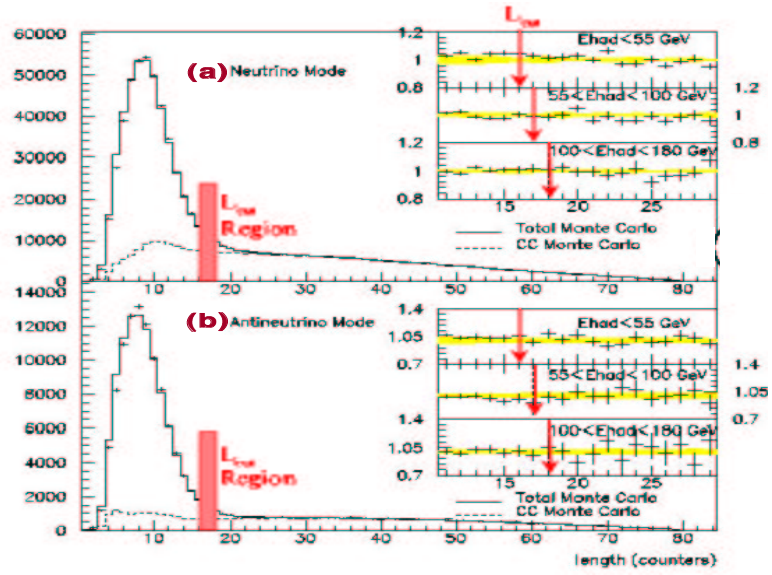

Figure 10: Length distributions of events in neutrino (a) and anti-neutrino running modes. The histograms represent MC predictions of CC (dashed) and the sum of CC and NC (solid) events.

verse direction. Finally, to ensure neutrino induced interactions and to better discriminate CC and NC events from each other, the longitudinal vertex of the event are required to be within the central 64 counters of the calorimeter. After these three selection cuts, the data sample consisted of 1.62×10^6 neutrino and 350,000 anti-neutrino events. Figure 9 shows the comparisons of neutrino (top) and anti-neutrino (bottom) fluxes in these events to MC predictions. The comparison indicates excellent agreement between data and MC. This flux distribution is then used as input to the detailed detector MC for extraction of $\sin^2\theta_W$.

5.2 Energy Dependent Length Cut

NuTeV decided to employ a hadronic energy-dependent length cut to maximize the statistics of the samples and to reduce systematic uncertainties. Figure 10 shows length distributions of selected events in neutrino (top) and anti-neutrino (bottom) running modes. The histograms represent MC predictions for CC events (dashed) and the sum of CC and NC (solid), while the crosses represent data points. The length cuts represented by a bar in the histograms are 16 for events with $55 \leq$

$E_{had} < 100$ GeV, 17 for $E_{had} < 55$ GeV and 18 for $100 \leq E_{had} < 180$ GeV. The plots in the insets show the comparisons between data and MC predictions in the cut region and demonstrate good agreement between data and MC within the systematic uncertainties. Using the variable length cut, the neutrino events have 457,000 short and 1.167×10^6 long events, resulting in the experimental ratio $\mathcal{R}_\nu^{exp} = 0.3916 \pm 0.0007$(stat.). Conversely, anti-neutrino events consist of 101,000 short and 250,000 long events, resulting in the ratio of from the anti-neutrino running mode, $\mathcal{R}_{\overline{\nu}}^{exp} = 0.4050 \pm 0.0016$(stat.).

5.3 Monte Carlo Prediction

In order to relate measured ratios of short to long events, $\mathcal{R}_\nu^{exp}$ and $\mathcal{R}_{\overline{\nu}}^{exp}$, to the actual values of $\sin^2\theta_W$, it is crucial to properly take into account all aspects of the experiment in the MC. Since some of the effects that must be taken into account rely heavily on MC predictions, instead of carrying out the analysis in experiment and in MC, NuTev integrates all the measured effects into the MC and relates them to the experimental measurements. The first such effects are the factors that contaminate events, thereby making long events look short or short events look long. The sources of contamination in short events are;

- Short ν_μ CC events due to the early exit of muons before they reach the muon spectrometer or range-outs due to kinematics. These effect are on the order of 20% for ν_μ and 10% for $\overline{\nu}_\mu$ events.
- Short ν_e CC events. Since electrons lose their energy immediately inside the steel calorimeter, all CC events from ν_e look exactly like short events. While the largest sources of uncertainty in ν_e flux have been eliminated in the beam, ν_e from charged hadron decays still makes into the detector. The flux of ν_e in the beam is estimated to be 5% for both the running modes, using $K_{e3}^{\pm}$ decays.
- Large angle cosmic ray events. While the fiducial cuts eliminates a large fraction of cosmic ray muon events coming from the top, due to inefficiencies in counters and other experimental factors, there is still some minimal amount of contamination from large angle cosmic ray muons. The contamination from this factor is estimated to be 0.9%, measured in data.

Conversely the sources of contamination in long events are:

Table 1: Itemization of experimental systematic effects, their estimated magnitudes and the tools NuTeV used to estimate the effects.

Effect	Magnitude ($\delta\sin^2\theta_W$)	Tools
Z_{Vert}	0.001/inch	dimuon ($\mu^+\mu^-$ events)
X_{Vert}, Y_{Vert}	0.001	MC
Counter Noise	0.00035	Testbeam Muons
Counter Efficiency	0.0002	ν_μ events
Counter Active Area	0.00025/inch	ν_μ CC and Testbeam
Hadron Shower Length	0.0015/cntr	Testbeam hadrons
Calorimeter Energy Scale	0.001/1%	Testbeam
Muon Energy Deposit	0.004	ν_μ CC events

- Long ν_μ NC events. Since the hadronic showers can fluctuate in the longitudinal direction via punch through effects or from in-flight decays of hadrons, NC events can be counted as long events. This effect is estimated to be 0.7% for both neutrino and anti-neutrino running modes.
- Hard Muon Bremstraahlung events. When the muons from upstream neutrino interactions in the shield traverse the material they can radiate high energy photons. These photons deposit all their energy at the time of emission, making the event look like a CC event. The level of this effect is estimated to be 0.2%.

The MC also must take into account other systematic effects that will impact the categorization of events. The remaining experimental effects are the vertex position resolution, counter active area and efficiencies (which most likely shorten the events), counter noise (which most likely lengthen the events), hadronic shower length simulation, muon energy deposition simulation, and the calorimeter energy scale. Table 1 shows the effect of each of these systematic uncertainty sources and the tools that NuTeV uses to estimate the uncertainties.

The flux of electron neutrinos can be constrained by neutrino events in anti-neutrino running mode in the charm and K_L–induced production of ν_e in the medium energy range ($80 < E_\nu < 180$ GeV). In addition, since the electrons from ν_e CC events deposit all their energy within a few counters of the interaction vertex, the shower shape analysis can provide direct measurement of ν_e events, though it is less precise due to the inherent position resolution of the crude calorimeter.

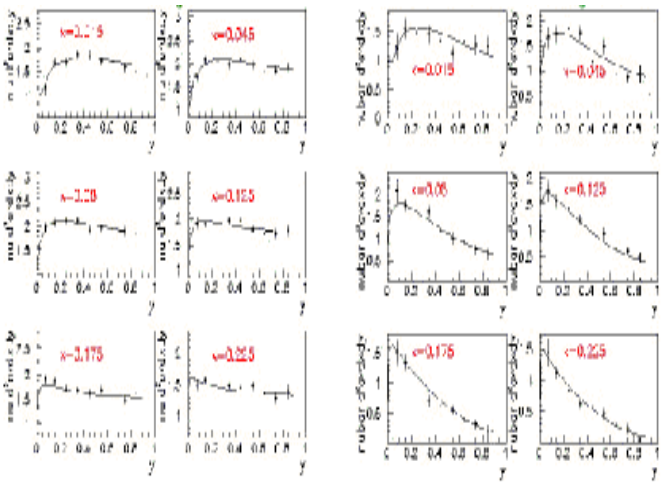

Figure 11: Measured cross sections of neutrino (left) and anti-neutrino (right) CC interactions from CCFR at $E_{\rm vis} = 190$GeV at various momentum fractions, x. The lines on the plots represent a PDF fit to the data.

The ratio of measured ν_e events to the MC prediction are 1.05 ± 0.03 for ν_e and 1.01 ± 0.04 for $\overline{\nu}_e$ events. NuTeV used the weighted average of these two ratios for its uncertainty estimate due to ν_e flux. This produced an uncertainty of 0.0005 in the measured ratio, $\mathcal{R}_\nu^{exp}$.

In order to take into account kinematic effects in the events, NuTeV used parton distribution functions measured in the previous incarnation of the NuTeV experiment, CCFR.[4,14] These effects are important to properly model crossover contamination from short ν_μ CC events. Figure 11 shows measured cross sections for neutrino (left) and anti-neutrino (right) CC interactions at $E_{\rm vis} = 190$ GeV for various momentum fractions, x. The lines on the plots represent PDF fit to the data that is used for the $\sin^2\theta_W$ analysis

Finally the MC also takes into account the fluxes of all neutrinos, ν_μ, ν_e, $\overline{\nu}_\mu$ and $\overline{\nu}_e$. The agreement between data and MC of the neutrino flux is shown in Fig. 9. The MC also includes shower length modeling based on continuous test beam hadron data to correct, in particular, for short events that appear long. The remaining effects, such as detector responses as a function of energy, position and time have been measured using the continuous test beam and are incorporated into the MC as well.

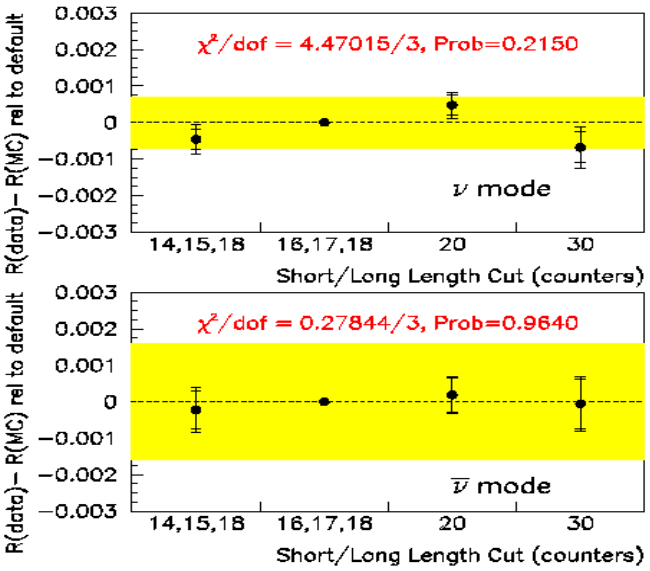

Figure 12: The difference between $\mathcal{R}_\nu^{exp}$ and $\mathcal{R}_\nu^{MC}$ as a function of length cut for neutrino (top) and anti-neutrino (bottom) running modes. The bands represent one standard deviation uncertainty.

It is crucial to verify the consistency of the primary variable, $\mathcal{R}_\nu^{exp}$ between data and MC under the changes in cuts and event variables. The longitudinal vertex cut variation checks the detector uniformity, the length cut checks the CC and NC crossover, the transverse vertex cut checks the NC background at the edge of the detector, and the visible energy (E_{had}) checks the detector energy scale and other factors. Figure 12 shows the difference between $\mathcal{R}_\nu^{exp}$ and $\mathcal{R}_\nu^{MC}$ as a function of length cut for neutrino (top) and anti-neutrino (bottom) running modes. The plots demonstrate an excellent agreement between MC and data throughout the variation in length cut, clearly showing the excellent stability of $\mathcal{R}_\nu^{exp}$. The bands indicate one standard deviation uncertainty.

6 Result of $\sin^2\theta_W$ from NuTeV

Using the MC which incorporates all experimental aspects of the measurement, NuTeV extracts $\sin^2\theta_W$ by performing fits to the measured ratios, $\mathcal{R}_\nu^{exp}$ and $\mathcal{R}_{\overline{\nu}}^{exp}$. As described in section 5.2, the measured ratios of NC to CC interactions are

$\mathcal{R}_\nu^{exp} = 0.3916 \pm 0.0007$ (stat.) for and $\mathcal{R}_{\overline{\nu}}^{exp} = 0.4050 \pm 0.0016$ (stat.) for the neutrino and anti-neutrino running modes, respectively. The fit is carried out using the Llewellyn-Smith formula in Eq. 6 which expresses $\mathcal{R}^{(\nu,\overline{\nu})}$ as a function of $\sin^2\theta_W$. The NuTeV fit is done simultaneously on $\mathcal{R}_\nu^{exp}$ and $\mathcal{R}_{overline\nu}^{exp}$ for $\sin^2\theta_W$ and m_c, and for $\sin^2\theta_W$ and ρ_0 independently. By employing this technique, NuTeV utilizes the fact that $\mathcal{R}^\nu$ is sensitive to $\sin^2\theta_W$ while $\mathcal{R}^{\overline{\nu}}$ is not. Therefore, effectively $\mathcal{R}^\nu$ is used to extract $\sin^2\theta_W$, and $\mathcal{R}^{\overline{\nu}}$ is used to control systematic uncertainties.

The result from a single parameter fit that uses SM values for electroweak parameters ($\rho_0 = 1$) yields:

$$\sin^2\theta_W = 0.2277 \pm 0.0013(\text{stat.}) \pm 0.0009(\text{syst.}), \tag{9}$$

with

$$m_c = 1.32 \pm 0.009(\text{stat.}) \pm 0.06(\text{syst.}), \tag{10}$$

using $m_c = 1.38 \pm 0.14\text{GeV/c}^2$ as input to the fit. The value of $\sin^2\theta_W$ from single parameter fit is about three standard deviations higher compared to the SM value. Performing a two parameter fit while floating the electroweak parameter ρ_0 yields:

$$\sin^2\theta_W = 0.2265 \pm 0.0031, \tag{11}$$

and

$$\rho_0 = 0.9983 \pm 0.040. \tag{12}$$

The uncertainty on $\sin^2\theta_W$ from the two parameter fit is dominated by systematic uncertainties, because the fit cannot take advantage of sea quark cancellations. The two parameter fit demonstrates that ρ_0 is consistent with SM predictions within the uncertainties, giving confidence in our extraction procedures. Table 2 shows $\sin^2\theta_W$ uncertainties due to various sources. As can be seen, the dominant uncertainty for this measurement is the statistical uncertainty of the data. The reduction of various previously dominant systematic uncertainties demonstrates that the combination of the new experimental setup and the technique to utilize the separate neutrino and anti-neutrino data to extract $\sin^2\theta_W$ has worked extremely well.

The final result from the NuTeV $\sin^2\theta_W$ measurement in the on-shell renormalization scheme is derived from the single parameter fit:

Table 2: Summary of uncertainties in the NuTeV $\sin^2\theta_W$ measurements.

SOURCE OF UNCERTAINTY	$\delta \sin^2\theta_W$
Statistical	**0.00135**
$\nu_e/\overline{\nu}_e$	0.00039
Event Length	0.00046
Energy Measurement	0.00018
TOTAL EXP. SYST.	0.00063
CC Production of Charm	0.00047
Higher Twist	0.00014
Non-Isoscalar Target	0.00005
Strange/Charm Sea	0.00036
$\sigma^\nu/\sigma^{\overline{\nu}}$	0.00022
Radiative Corrections	0.00011
Longitudinal Structure Function, R_{L}	0.00032
TOTAL PHYSICS MODEL	0.00070
TOTAL UNCERTAINTY	0.0022

$$\sin^2\theta_W{}^{(on-shell)} = 0.2277 \pm 0.0013(\text{stat}) \pm 0.0009(\text{syst}) \quad (13)$$
$$-0.00022 \times (\frac{M_t^2 - (175\text{GeV})^2}{(50\text{GeV})^2}) + 0.00032 \times ln(\frac{M_H}{150\text{GeV}}).$$

The small residual dependence of this result on M_{top} and M_H comes from the leading terms in the electroweak radiative corrections.[15]

Since, within the on-shell renormalization scheme, $\sin^2\theta_W$ is related to M_W and M_Z and combined with the standard model prediction of $\rho_0 = 1$ yields $\sin^2\theta_W \equiv 1 - \frac{M_W^2}{M_Z^2}$. This result is equivalent to:

$$M_W = 80.14 \pm 0.08(\text{GeV/c}^2) \quad (14)$$

Figure 13 shows comparisons of the above value to the other direct measurements. As the figure shows, the NuTeV result is about three standard deviations lower than the world average and is as precise as the measurements from the Tevatron collider experiments.

Figure 14 shows 68% to 99% confidence level contours of the results from the two parameter fit in Eq. 11. The green solid circle represents the SM prediction of ρ_0 and $\sin^2\theta_W{}^{(on-shell)}$. As the mass of the top quark and the Higgs boson vary, the central value moves around slightly to fit one or the other of the two parameters. However, both ρ_0 and $\sin^2\theta_W{}^{(on-shell)}$ simultaneously agreeing with the SM prediction is very unlikely. The global electroweak fit performed by the CERN electroweak working group[16] demonstrates a reduced χ^2 of 29.7/15 ($\mathcal{P} = 1.3\%$) and 20.5/14 ($\mathcal{P} = 11.4\%$) with and without incorporating the NuTeV $\sin^2\theta_W$ result. By incorporating the NuTeV result, the confidence level on the upper limit of M_{Higgs} weakens slightly.

A model-independent analysis was also performed through the fit to the left and right-handed light quark couplings (g_L and g_R). For an isoscalar target the neutrino-nucleon couplings are expressed as:

$$g_L^2 = u_L^2 + d_L^2 = \rho_0^2(\frac{1}{2} + \sin^2\theta_W + \frac{5}{9}sin^4\theta_W) \quad (15)$$
$$g_R^2 = u_R^2 + d_R^2 = \rho_0^2\frac{5}{9}sin^4\theta_W. \quad (16)$$

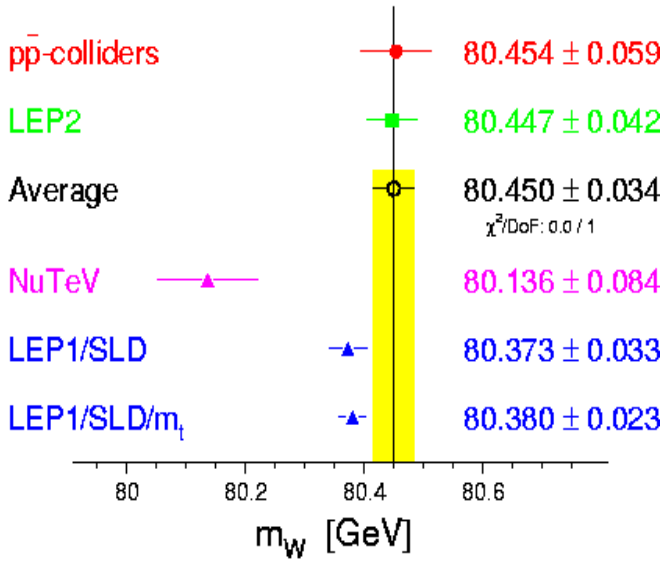

Figure 13: Various measurements of M_W.

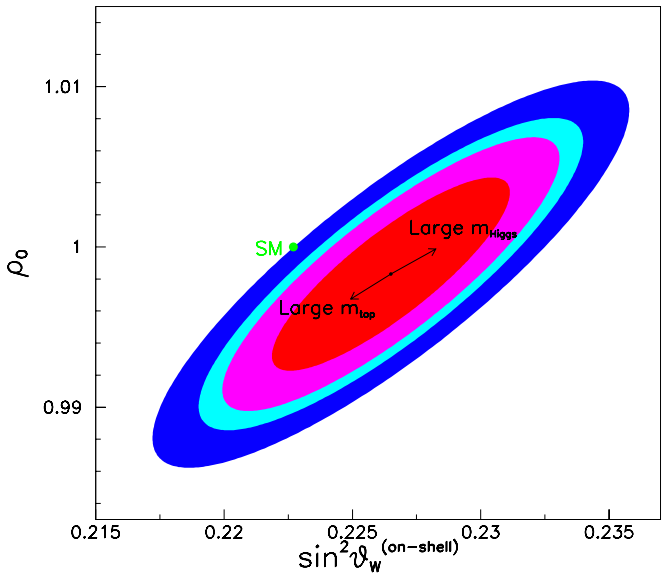

Figure 14: Confidence level contour plots for 68% to 99% of rho_0 and $\sin^2\theta_W{}^{(on-shell)}$ from the two parameter fit.

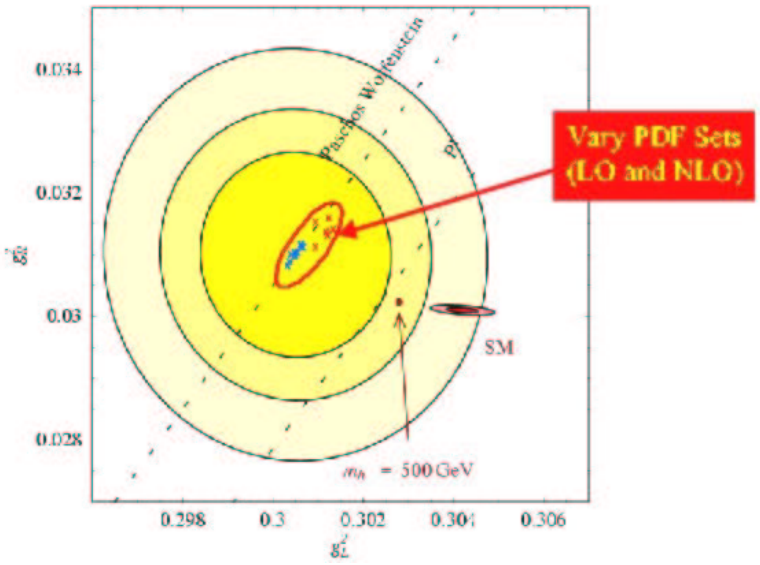

Figure 15: Confidence level contours for right (g_R^2) vs left-handed (g_R^2) light quark couplings from the model independent analysis. The crosses in the center of the contour show the variation of these couplings for leading and next-to-leading order PDF sets.

By performing a two parameter fit of g_L and g_R to the measured ratios, $\mathcal{R}_\nu^{exp}$ and $\mathcal{R}_{overline\nu}^{exp}$, NuTeV obtains:

$$g_L^2 = 0.3005 \pm 0.0014, \tag{17}$$

$$g_R^2 = 0.0310 \pm 0.0011. \tag{18}$$

The predictions for these couplings from the SM are $g_L^2 = 0.3042$ and $g_R^2 = 0.0301$. Thus, the left-hand coupling lies approximately -2.6 standard deviations away from the SM predictions, while the right-hand coupling seems to agree well.

Figure 15 shows various confidence level contours for these results. The crosses in near the central value of the measurement are our attempt to explain the deviation by the variation in leading and next-to-leading order PDF's.

7 Possible Interpretations

The natural question to be asked regarding the $\sin^2\theta_W$ result from NuTeV is: what are the possible interpretations of this discrepancy from the SM prediction?

There are two large categories of interpretations, one based on known physics effects and the other on new physics.

The ones based on existing physics are as follows:

- The $\mathcal{R}^{\nu}$ technique is sensitive to q vs. $\overline{q}$ differences and to higher-order effects. In other words, the technique is susceptible to differences in valence quark and anti-quark momentum distributions in the target protons or neutrons.[17–20] First of all, NuTeV does not exactly measure R^{-}, in part, because it is not possible to measure neutral current reactions down to zero recoil energy. A numerical evaluation of the isospin asymmetry effect[21] shows that the level of isospin violation required to shift the $\sin^2\theta_W$ would be as much as 5% of the sum of valence u in proton and d quark in neutron and that for strange sea would be about 30% of the total s quark contents.
- The assumption of isospin symmetry in the target, even after correction, might not be entirely correct. The isospin symmetry violation is expected to be at the level of 1%. NuTeV reduces this effect by about a factor of three, using the ratio of ν and $\overline{\nu}$ cross sections.
- Strange quark and anti-strange quark momentum distributions of the target might not be symmetric.[22] In other words, the total number of s and $\overline{s}$ might be the same but the momentum distributions could differ. A value of $\Delta s = s - \overline{s} \sim +0.002$ could shift $\sin^2\theta_W$ by -0.0026, thereby accounting for half the discrepancy.[20] NuTeV measures strange quark content directly from the experiment using dimuon final states with two opposite charge muons. This measurement shows that $\Delta s << 0.002$.[21]
- Higher-order and PDF effects might cause the discrepancy. However, these effects are too small to account for such a large discrepancy, as it has been demonstrated in the previous section.
- Heavy vs. light target effect.[23] Since most the data used for the PDF fit come from deep inelastic scattering experiments that use a light target, the difference in target mass can cause the discrepancy. GIven that NuTeV used PDF's measured from CCFR extracted from the same target, this cannot be a factor for the discrepancy.

The explanations based on new physics and other reasons are as follows:

- Change in coupling strength due to the exchange of heavy non-SM vector

bosons, such as Z', lepto-quarks, etc.[24,25]

- Propagators and coupling corrections are too small to account for the discrepancy.
- MSSM (Minimal Supersymmetric extension of Standard Model) loop corrections are not only the wrong sign relative to the effect but also are too small compared to the discrepancy.
- Gauge boson interactions allow generic couplings. However LEP and SLAC results shows that this effect should be less than 10^{-3}.

In addition to the above possible interpretations, many others have been proposed. However, so far there has not been any interpretation that can fully explain this discrepancy.

8 Future

The NuTeV detector was dismantled in 1999 to make room for other experiments at Fermilab. At present there is no other experiment that can perform a measurement of $\sin^2\theta_W$ using the techniques, described in this paper. Since muons undergo weak decay resulting in $\nu_\mu\overline{\nu}_e e^-$, a new storage ring facility that stores a large number of muons can provide an extremely high flux neutrino beam that is both pure and well understood and is extremely pure. While development toward such facility is in progress at several high energy physics laboratories around the world, such a facility is still ten to fifteen years away in the future, leaving the experimental verification of the NuTeV discrepancy open.

9 Conclusions

NuTeV has performed a precision measurement of $\sin^2\theta_W$, using the SSQT that allowed the experiment to measure the ratio of neutral and charged current cross sections in neutrino and anti-neutrino beams separately. This allowed the experiment to utilize $\mathcal{R}_\nu^{exp}$ and $\mathcal{R}_{\overline{\nu}}^{exp}$ to extract ${\sin^2\theta_W}^{(on-shell)}$ with significantly reduced systematic uncertainties. The final result for $\sin^2\theta_W$ from the one parameter fit yields:

$$\sin^2\theta_W = 0.2277 \pm 0.0013(\text{stat.}) \pm 0.0009(\text{syst.}). \tag{19}$$

This result corresponds to a mass of the W boson:

$$M_W = 80.14 \pm 0.08 \ (\mathrm{GeV/c^2}). \tag{20}$$

The NuTeV result deviates from the SM prediction by about three standard deviations.[28] A model-independent analysis to light quark couplings shows the left-hand coupling is lower than the SM prediction by 2.6 standard deviations, while the right-hand coupling is in agreement with SM. This discrepancy in $\sin^2\theta_W$ from the SM has generated significant interest in the community. However no single hypothesis is able to explain the discrepancy in a satisfactory manner. While the cause for the discrepancy is still unknown and it is possible that this discrepancy could be a statistical fluctuation, it nonetheless provides exciting new possibilities for new physics. Unfortunately, since the NuTeV detector was dismantled in 1999 and there is no other existing experiment which is equipped to perform this measurement, this discrepancy will remain a puzzle experimentally. A new accelerator facility such as a muon storage ring, has the potential to provide an extremely clean and well understood neutrino beam to perform this measurement in the future.

References

[1] S. Weinberg, Rev. Mod. Phys. **52**, 515 (1980).

[2] W.K. Sakumoto *et. al.*, Nucl. Inst. Meth. **A294**, 179 (1990).

[3] C.H.Llewellyn Smith, Nucl. Phys. **B228**, 205 (1983)

[4] B.E.Seligman *et al.*, CCFR Collaboration, Phys. Rev. Lett. **79**, 1213 (1997); B. T. Fleming *et al.*, CCFR/NuTeV Collaboration, Phys. Rev. Lett. **86**, 5430 (2001)

[5] L.W. Whitlow, *SLAC–Report–*357, 109 (1990).

[6] C.Arroyo, B.J.King *et. al.*, Phys. Rev. Lett. **72**, 3452 (1994).

[7] K.S.McFarland *et al.*, CCFR, Eur. Phys. Jour. **C1**, 509 (1998)

[8] Slow rescaling paper

[9] S.A.Rabinowitz *et. al.*, Phys. Rev. Lett. **70**, 143 (1993); M Goncharov *et al.*, NuTeV Collaboration, Phys. Rev. **D64**, 112006 (2001)

[10] A.Romosan *et. al.*, Phys. Rev. Lett. **78**, 2912 (1997).

[11] E.A.Paschos and L. Wolfenstein, Phys. Rev. **D7**, 91 (1973)

[12] J. Yu *et al.*, NuTeV Collaboration, "NuTeV SSQT Performance," Fermi-TM-2040, Unpublished (1998)

[13] D. Harris, J. Yu *et al.*, NuTeV Collaboration, Nucl. Instrum. Meth. **A447**, 377 (2000)

[14] U.K.Yang *et al.*, CCFR/NuTeV Collabortion, Phys. Rev. Lett. **87**, 251802 (2001)

[15] D.Yu. Bardin, V.A. Dokuchaeva, JINR-E2-86-260 (1986)

[16] The LEP Electroweak Working Group home page:
`http://lepewwg.web.cern.ch/LEPEWWG/Welcome.html`

[17] E. Sather, Phys. Lett. **B274**, 433 (1992)

[18] E. N. Rodionov, A. W. Thomas, and J. T. Londergan, Mod. Phys. Lett. **A9**, 1977 (1994)

[19] F. Cao and A. I. Signal, Phys. rev. **C62**, 015203 (2000)

[20] S. Davison, S. Forte, P. Gambino, N. Rius, and A. Strumia, hep-ph/0112302 (2002)

[21] Z.P. Zeller *et al.*, NuTeV Collaboration, Phys. Rev. **D65**, 111103 (2002)

[22] A.I. Signal and A. W. Thomas, Phys. Lett. **B191**, 205 (1987); M. Burkardt and B. J. Warr, Phys. Rev. **D45**, 958 (1992); S. Brodsky and B. Ma, Phys. Lett. **B381**, 317 (1996); W. Melnitchouk and M. Marheiro, Phys. Lett. **B451**, 224 (1999)

[23] S. Kovalenko *et al.*, hep-ph/0207158 (2002)

[24] R. Casalbuoni, S. De Curtis, D. Dominici and R. Gatto, Phys. Lett. **B460**, 135 (1999); J. L. Rosner, Phys. Rev. **D61**, 016005 (2000); A. Bodek and u. Baur, Eur. Phys. Jour. **C21**, 607 (2001)

[25] J. Erler and P. Langacker, Phys. Rev. Lett. **84**, 212 (2000)

[26] G. C. Cho, K. Hagiwara and Y. Umeda, Nucl. Phys. **B531**, 65 (1998);

[27] D. Zeppenfeld and K. Cheung, hep-ph/9810277 (1998)

[28] G. P. Zeller, K. S. McFarland *et al.*, NuTeV Collaboration, Phys. Rev. Lett. **88**, 091802 (2002)